Biochimica et Biophysica Acta 1848 (2015) 1203–1211

Contents lists available at ScienceDirect

Biochimica et Biophysica Acta

journal homepage: www.elsevier.com/locate/bbamem

Reduced graphene oxide directed self-assembly of phospholipid monolayers in liquid and gel phases

Longfei Rui [a,b], Jiaojiao Liu [a,b], Jingliang Li [d], Yuyan Weng [a,b], Yujiang Dou [a,c], Bing Yuan [a,b,*], Kai Yang [a,b], Yuqiang Ma [a,b,e,**]

[a] Center for Soft Condensed Matter Physics and Interdisciplinary Research, Soochow University, Suzhou, 215006, PR China
[b] College of Physics, Optoelectronics and Energy, Soochow University, Suzhou, 215006, PR China
[c] School of Electronic and Information Engineering, Soochow University, Suzhou, 215006, PR China
[d] Institute for Frontier Materials, Deakin University, Waurn Ponds, Vic, 3216, Australia
[e] National Laboratory of Solid State Microstructures and Department of Physics, Nanjing University, Nanjing, 210093, PR China

ARTICLE INFO

Article history:
Received 8 December 2014
Received in revised form 10 February 2015
Accepted 16 February 2015
Available online 24 February 2015

Keywords:
Reduced graphene oxide
Self-assembly
Phospholipid monolayer

ABSTRACT

The response of cell membranes to the local physical environment significantly determines many biological processes and the practical applications of biomaterials. A better understanding of the dynamic assembly and environmental response of lipid membranes can help understand these processes and design novel nanomaterials for biomedical applications. The present work demonstrates the directed assembly of lipid monolayers, in both liquid and gel phases, on the surface of a monolayered reduced graphene oxide (rGO). The results from atomic force microscopy indicate that the hydrophobic aromatic plane and the defect holes due to reduction of GO sheets, along with the phase state and planar surface pressure of lipids, corporately determine the morphology and lateral structure of the assembled lipid monolayers. The DOPC molecules, in liquid phase, probably spread over the rGO surface with their tails associating closely with the hydrophobic aromatic plane, and accumulate to form circles of high area surrounding the defect holes on rGO sheets. However, the DPPC molecules, in gel phase, prefer to form a layer of continuous membrane covering the whole rGO sheet including defect holes. The strong association between rGO sheets and lipid tails further influences the melting behavior of lipids. This work reveals a dramatic effect of the local structure and surface property of rGO sheets on the substrate-directed assembly and subsequent phase behavior of the supported lipid membranes.

1. Introduction

With the striking progress in nanotechnology, extensive attention has been focused on the applications of nanomaterials in biomedical fields. Biological responses of biosystems to the implant of biomaterials significantly determine the effect and even safety/cytotoxicity of them. A large number of researches have reported that the physical and surface chemical properties of biomaterials, such as their hydrophobic/hydrophilic property and surficial topographies, would significantly influence the cellular behaviors including cellular uptake and the consequent intracellular location and translocation of nanomaterials [1–4]. In addition, cell functioning is, to a large extent, dependent on the extracellular matrix (ECM) environment. It has been established that local physical environment modulates many cell responses, including cell migration, proliferation, and cytoarchitecture [5–7]. However, these modulations are probably cell-type dependent. On the other hand, cell membranes, composed of a basic lipid bilayer platform with incorporated functional proteins, are primarily involved in regulation of these biological processes including regulation of response to the extracellular matrix. Therefore, a fundamental understanding of the interactions between lipid membranes and biomaterials at a molecular level can contribute to the understanding of these processes and development of biomedical applications of nanomaterials [8–10]. Previous studies have shown that subtle differences at the membrane interface with the substrate translate into dramatic differences in lateral fluidities and phase separation in supported lipid membranes [11]. Despite this, a better understanding of the dynamic assembly and environmental response of lipid membranes, which are composed of two asymmetric leaflets of lipid monolayers, is still needed.

In recent years, carbon-based materials, including carbon nanotubes and graphene (or reduced graphene oxide), have been considered attractive candidates for various biomedical applications such as scaffolds in tissue engineering, near-infrared biomedical imaging [12], substrates for stem cell differentiation [13], and surficial coverage of implant

* Correspondence to: B. Yuan, Center for Soft Condensed Matter Physics and Interdisciplinary Research, Soochow University, Suzhou, 215006, PR China. Tel./fax: +86 512 65220239.
** Correspondence to: Y. Ma, College of Physics, Optoelectronics and Energy, Soochow University, Suzhou, 215006, PR China. Tel./fax: +86 25 83592900.
E-mail addresses: yuanbing@suda.edu.cn (B. Yuan), myqiang@nju.edu.cn (Y. Ma).

http://dx.doi.org/10.1016/j.bbamem.2015.02.018
0005-2736/

devices [14]. Recently, many researches have been worked on the cellular responses to carbon-based nanomaterials [15–17]. For example, fibroblasts and HeLa cells were reported to proliferate well on substrates coated with graphene, graphene oxide or carbon-nanotube, which suggests that such carbon-coated surface might be a suitable substrate for cell culturing applications [16]. However, another work found that the self-spreading of supported lipid bilayer on a SiO_2 surface was blocked by graphene oxide pieces [18]. In this context, a fundamental and systematic investigation on interfacial interactions between phospholipid and graphene on a molecular level is needed, which might promise faster and smarter exploitation of the distinct characteristics of graphene for biological applications. Furthermore, incorporation of lipids with graphene provides an important way for preparing multifunctional hybrid materials for biosensing [19,20], drug delivery [21], and photochemical catalysis [22].

Atomic force microscopy (AFM) has been an essential tool to investigate the topology of supported lipid mono/bilayers due to its high sensitivity and localization [23]. In this work, we take advantage of AFM technique to investigate the directed self-assembly of phospholipid molecules, in both liquid and gel phases, in response to the surface features of monolayered rGO sheets that are supported on a mica surface. Results show that subtle structural details in rGO substrate are amplified into dramatic differences in morphology and lateral fluidity in supported lipid monolayers. To the best of our knowledge, this work reports the first experimental evidence highlighting the effect of local topography of rGO surface and lipid phase on the molecular assembly of lipid monolayers. It provides a new framework for understanding the cell membrane responses to rGO and help design novel rGO/lipid nanocomposite biomaterials.

2. Materials and methods

2.1. Chemicals

1,2-Dioleoyl-*sn*-glycero-3-phosphocholine (DOPC), 1,2-dipalmitoyl-*sn*-glycero-3-phosphocholine (DPPC), and 1,2-dipalmitoyl-*sn*-glycero-3-phosphoethanolamine-N-(lissamine rhodamine B sulfonyl) (Rh-PE) were purchased from Avanti Polar Lipids and used as received. Graphene oxide (2 mg mL^{-1}, dispersion in water) and 1-Oleoyl-rac-glycerol (MO) were purchased from Sigma-Aldrich. Sheet mica and chloroform (99.7%) were purchased from Shanghai Chemical Reagents Company.

2.2. Preparation of rGO sheets on mica

Supported graphene oxide (GO) flakes on mica were first prepared. A volume of 10 μL graphene oxide dispersion, with a concentration of 0.004 mg mL^{-1}, was dropped onto a freshly cleaved mica surface (8 × 8 mm) with a pipette and the solvent was allowed to evaporate slowly in a chamber. After complete evaporation, supported GO flakes were obtained. The sample was then annealed in Ar/H_2 at 450 °C for 30 min for reduction of GO to rGO, which was used for the following characterizations and lipid depositions [24].

2.3. Lipid monolayer deposition through Langmuir–Blodgett technique

A KSV NIMA Langmuir–Blodgett Deposition Trough (KN2002), with a useful surface area of 273 cm^2, was used to prepare lipid films. The lipids were first dissolved in chloroform to 0.2 mg mL^{-1} (1.0 mg mL^{-1} for MO). A volume of 8 μL lipid solution was spread onto the water/air interface in the trough. After evaporation of chloroform, the lipid layer was transferred by lifting the substrate vertically from the aqueous subphase, at a speed of 3 mm min^{-1}, while maintaining the surface pressure constant at the desired setpoint. A surface pressure of 32 mN m^{-1} was selected for the conventional lipid monolayer deposition (unless otherwise stated) as this value is low enough to prevent the monolayer to collapse, and high enough for a condensed state of the monolayer [25]. A much lower surface pressure of 15 mN m^{-1} was also used for control experiments. For the fluorescence experiments, 0.5 mol.% Rh-PE was added to the lipid solution in advance.

2.4. Characterizations

AFM images were collected with an Asylum Research MFP-3D-SA atomic force microscope (Santa Barbara, CA) setup in tapping mode in air. In the heating experiment, the temperature of the system was modulated and maintained at 60 °C with the original temperature control components from AR. The fluorescent image was taken on a Zeiss LSM 710 inverted confocal fluorescence microscope. All the experiments were carried out at room temperature of 22 °C.

3. Results and discussion

3.1. Fabrication of supported rGO sheets

Scheme 1 presents the molecular structure of the three types of lipids used in this work. In brief, DOPC consists of two unsaturated hydrocarbon tails in addition to the phosphor-nitrogen headgroup, while DPPC has two saturated hydrocarbon tails. Therefore, the melting temperature of DOPC (−20 °C) is much lower than that of DPPC (41 °C) [26]. At room temperature, they exist in liquid crystalline and gel phases, respectively. MO has a similar amphiphilic structure, being composed of a single unsaturated hydrocarbon chain bonded to a glycerol head by an ester bond [27].

For reference, we firstly prepared DOPC, DPPC and MO monolayers on neat mica surfaces by LB technique. The obtained lipid films are defect free and looked quite flat as shown in Figure S1, except that little cracks occurred on DPPC film due to gel phase [28]. To confirm the presence of the lipid films on the mica surfaces, 0.5 mol.% fluorescent Rh-PE lipid was pre-mixed with all the three lipids. Under confocal fluorescence microscopy, homogeneous distribution of fluorescence was found over surfaces of all the three samples (cf. Figure S2a). Due to the super-hydrophilic feature of mica surface (cf. Figure S3), the lipid molecules are supposed to assemble into a monolayer with hydrophilic headgroups fronting on the mica surface while the hydrophobic tails orienting towards the air.

On the other hand, we fabricated GO sheets supported on mica surface by the conventional drop-coating method. Under AFM characterizations as shown in Fig. 1a, the GO sheets were found spread on the mica surface, probably in a monolayer, with a size of a few micrometers. The surficial coverage of the GO sheets on mica can be modulated from below 20%, mostly monolayered, to more than 90%, mainly overlapped, by controlling the volume of GO dispersion dropped on mica. A single GO sheet has a thickness of 0.95 ± 0.05 nm as shown in the height profile in Fig. 1d. This agrees with the previous reports [29,30]. Meanwhile,

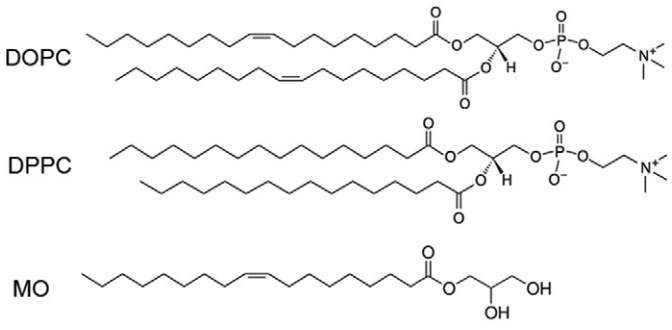

Scheme 1. Molecular structures of DOPC, DPPC and MO.

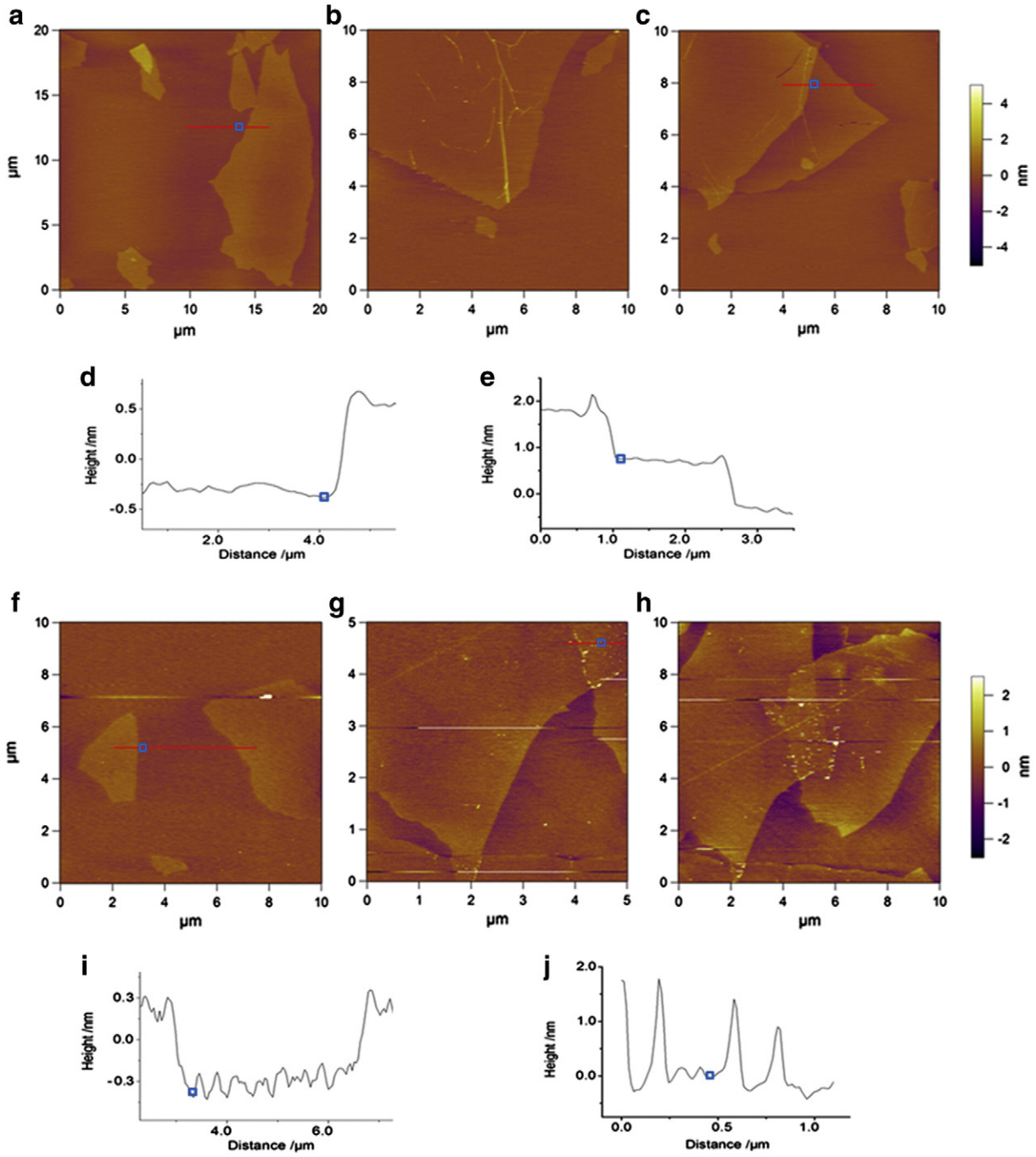

Fig. 1. Typical AFM images of GO (a–c) and rGO (f–h) flakes on mica, showing the flat surface of the sheets (a, f), including wrinkles and overlapped regions (b, c, g and h). Panels (d) and (e) are height profiles along the red lines in panels (a) and (c). Panels (i) and (j) are height profiles along the red lines in panels (f) and (g), corresponding to the thickness of a single rGO sheet and the roughness of the overlapped region, respectively. White lines in panels (f)–(g) are due to noise during scanning or impurities on the sample surface.

creasing and overlapping of GO sheets also occurred (Fig. 1b and c), while each layer of GO sheet maintained the intrinsic thickness of about 1 nm (Fig. 1e).

Through annealing in Ar/H_2 at a high temperature, GO can be reduced to rGO [31]. Fig. 1f presents AFM images of rGO sheets obtained, still being supported on mica. The flat surface of the GO sheets was maintained on rGO, while the thickness of the sheets has been decreased to 0.54 ± 0.05 nm (Fig. 1f and i). After reduction, the wrinkles of the GO sheets can still be distinguished. Moreover, the overlapping region of GO has been changed to plotted region with high roughness, of about 1.60 ± 0.15 nm (Fig. 1j).

3.2. Lipid monolayers on rGO surface

3.2.1. DOPC@rGO Film

The conventional LB technique was used to deposit condensed lipid monolayer on supported rGO surface with a constant surface pressure of 32 mN m^{-1}, which is considered the lateral pressure values in

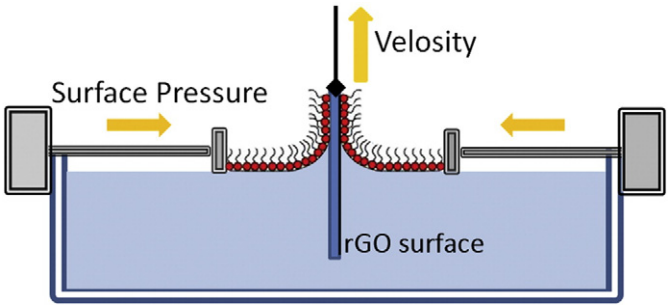

Scheme 2. Schematics of the experimental LB deposition of a lipid monolayer on an RGO covered mica surface.

liposomes (Scheme 2). During the film fabrication process, the rGO sheets were maintained on the mica surface stably. After transferring the lipids from the air–liquid interface to the solid surface, the subsequent solvent evaporation drives the self-assembly of lipid monolayer on the rGO surface, named DOPC@rGO film here. The surface topography of the film was then characterized with AFM. Fig. 2 shows the DOPC monolayers supported by rGO sheets on mica. Outlines of rGO sheets on mica can still be clearly distinguished. Furthermore, on the rGO regions, defect holes are obviously observed (Fig. 2a–c). For each hole, a circle of molecules or atoms, with a pronounced height compared with the other regions, is located surrounding the hole. In contrast, the other regions on the rGO sheets have a much lower roughness (Fig. 2d–f). The MO@rGO film was prepared in the same way and demonstrated a topography similar to that of the DOPC@rGO film (cf. Figure S4).

The size distribution of the holes on DOPC@rGO films is concluded in Figure S5, with an average diameter of 0.11 μm. The rising of the holes may be attributed to the defects on graphene planes due to the removal of oxygen functional groups during GO reduction process, which has been observed with atomic resolution aberration-corrected TEM technique [24,32]. To the best of our knowledge, this is the first time to

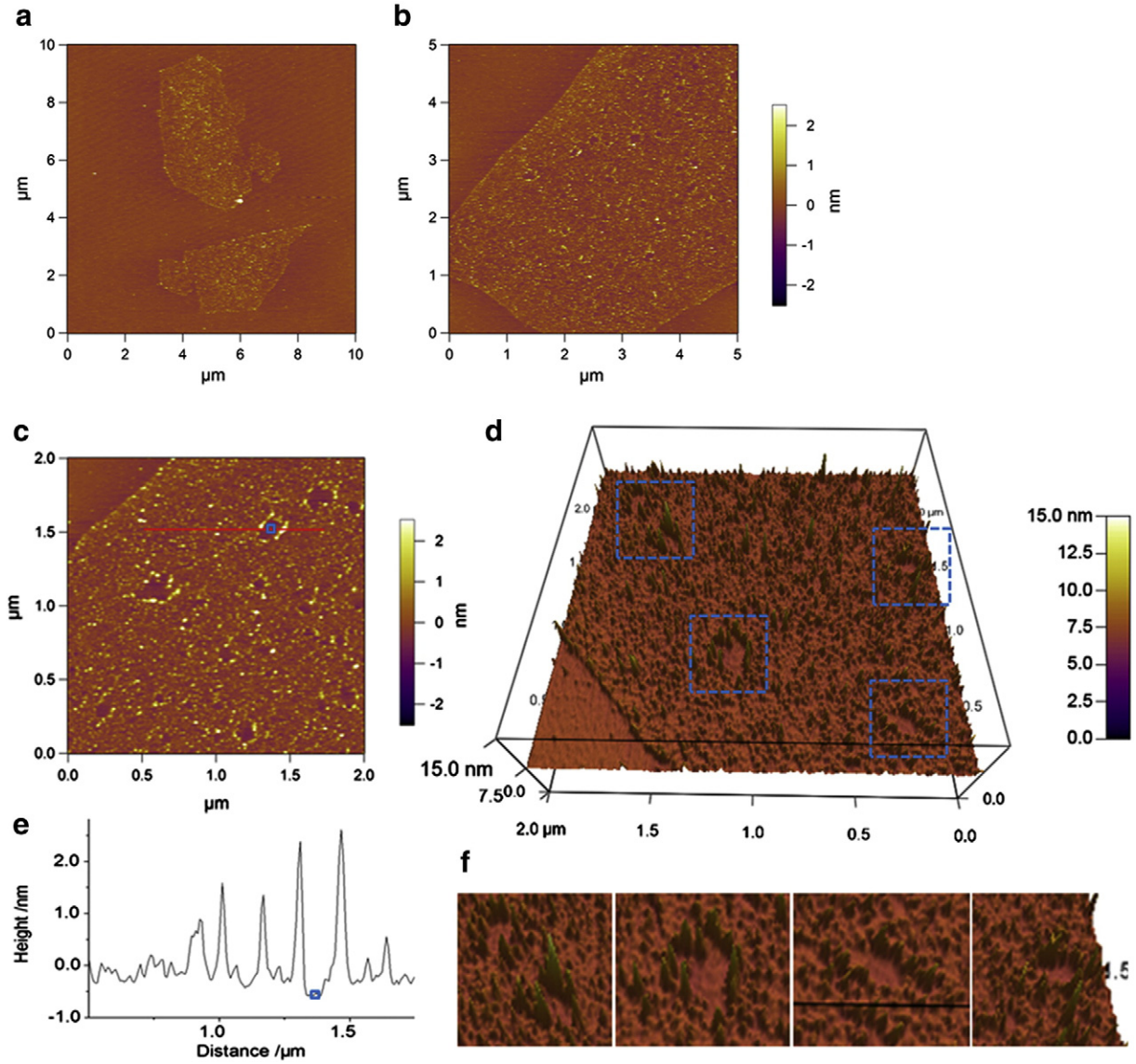

Fig. 2. AFM topographies of DOPC monolayers supported on rGO sheets. Panels (a) and (b) stand for different regions of a sample; panel (c) is a zoom in image of a portion of panel (b) within a 2 × 2 μm range; panel (d) is a pseudo-3D representation of panel (c). Panel (e) shows height profile along the red line in panel (c). Panel (f) shows enlargements as marked with blue dotted squares in panel (d), showing the pores and surrounding peaks around the pores on the rGO sheet. The surface pressure during the DOPC monolayer deposition was set at 32 mN m^{-1}.

observe the defective hole configuration of rGO sheets with AFM, due to the amplification of surfactant molecules. It is noted that the surface of the neat rGO sheets is absolutely flat under AFM observations (Fig. 1f). Therefore, such a circle of pronounced high area around each hole is supposed to be attributed to the assembly of phospholipid molecules, probably standing by or accumulations. This phenomenon is consistent with the lateral location of Au nanoparticles surrounding the defect edges of lipid patches when the nanoparticles interact with supported lipid bilayers [33]. On the other hand, it is known that the surface of rGO sheets is quite hydrophobic due to aromatic rings of the scaffold plane of graphene. The hydrophobic tails of lipid molecules, rather than the hydrophilic heads, prefer to associate with the rGO sheets. Furthermore, DOPC exists in a liquid phase with significantly disordered tails at room temperature. Therefore, on the other regions of the rGO sheets besides the holes, it is probable that the hydrophobic tails of DOPC molecules spread over the hydrophobic surface of the aromatic plane in a completely random orientation, resulting in a lower height of the molecular layer compared with the pronounced molecular accumulations around holes.

It is reasonable to suppose that on the naked mica surface without rGO coverage, DOPC monolayers still exist. This is also confirmed by the homogeneous distribution of fluorescence of the DOPC@rGO film under confocal fluorescent microscope (cf. Figure S2b). However, because of the super-hydrophilic surface of mica, the lipids would assemble differently from that on the rGO surface. They prefer to locate with the headgroups associating with the mica surface while the tails orienting to the air [34]. From the height profile shown in Fig. 2e it is found that the hole bottom is even 0.2 nm lower than that of the mica surface (including the deposited lipid layer), which indicates that the lipids in the holes assembled in a way different from those on the outside mica surface, or even there is no lipid molecule within holes at all. As a result, in the following discussions of this work, we take the bottom of the holes as reference to judge the height of the other part of the samples.

3.2.2. DPPC@rGO film

In prominent contrast, the DPPC@rGO films, prepared by the same method as the DOPC and MO@rGO films, show different topographies. The DPPC monolayers cover the rGO surfaces completely, without any pores observed (Fig. 3). Despite this, the DPPC film on rGO is not as flat as that on mica. The height of lipid membrane on rGO surface is 1.8 nm higher than that on the mica surface, and the DPPC@rGO film has a roughness of less than 1 nm (Fig. 3d). It is indicated that a continuous membrane of DPPC monolayer, without the existence of holes, formed over the rGO surface. This might be because DPPC is in gel phase at room temperature, with the tails densely packed and orienting parallel to the film normal. The planar area per lipid molecule of the gel phase was reported to be 48 $Å^2$, compared with that of the liquid phase of 64 $Å^2$ [26]. The densely packing of the gel lipids leads to a much higher value of order parameter and also the blocked exchange bending constant [23,26]. Therefore, the planar geometry of lipid membrane in gel phase is much more stable and integrated than that in liquid phase. Therefore, hole defects were not present in the DPPC films.

3.3. Lipid monolayers on rGO surface with lowered surface pressure

We decreased the surface pressure during LB depositions of lipid membranes from 32 mN m^{-1} to 15 mN m^{-1}, while kept the other experimental conditions unchanged. In this case, the lipids are much more sparsely separated and the planar area per lipid molecule of DOPC and DPPC has increased to 83 and 51 $Å^2$, respectively, due to the decreased lateral pressure [35]. Figs. 4 and 5 present the AFM topographies of DOPC and DPPC monolayers as deposited, on supported rGO sheets on mica surface (named DOPC′@rGO and DPPC′@rGO, respectively). It is observed that the DOPC film emerges similar to the conditions at 32 mN m^{-1}. Holes, surrounded by molecules with a height of 1.86 ± 0.1 nm, distribute randomly over this DOPC′@rGO film surface. The roughness of the other regions on the film is much lower, with an

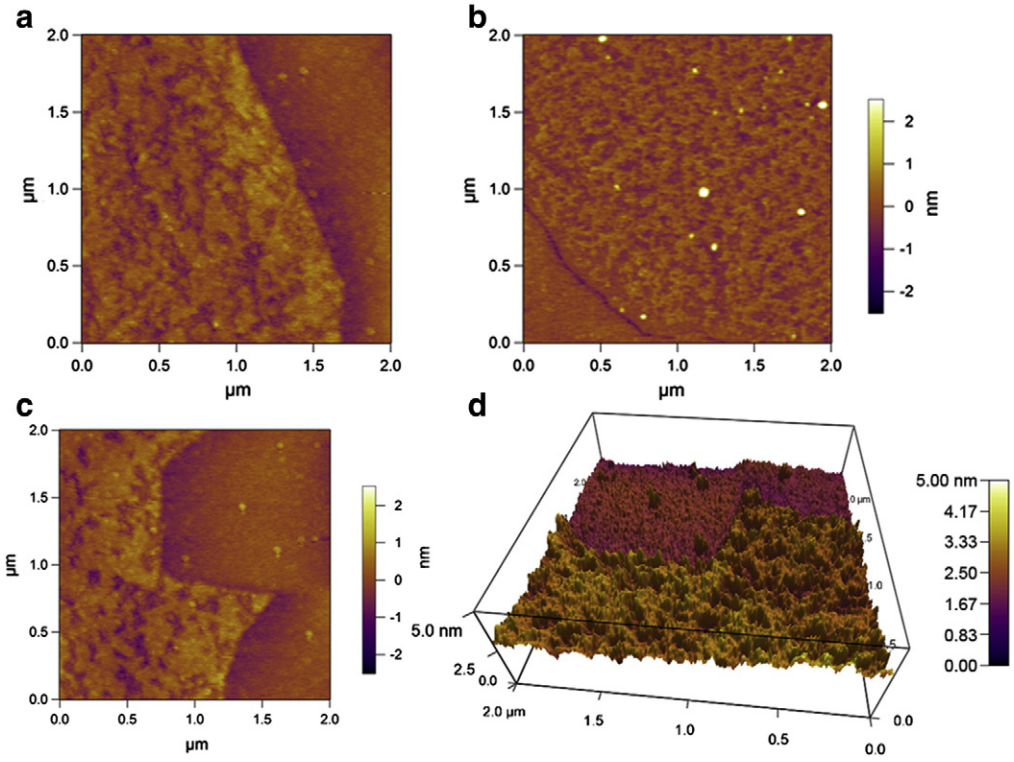

Fig. 3. AFM image of defect-free DPPC monolayers supported on rGO sheets. Panels (a)–(c) stand for different regions of samples; panel (d) is a 3D height mode image of panel (c). The surface pressure during film deposition was kept at 32 mN m^{-1}.

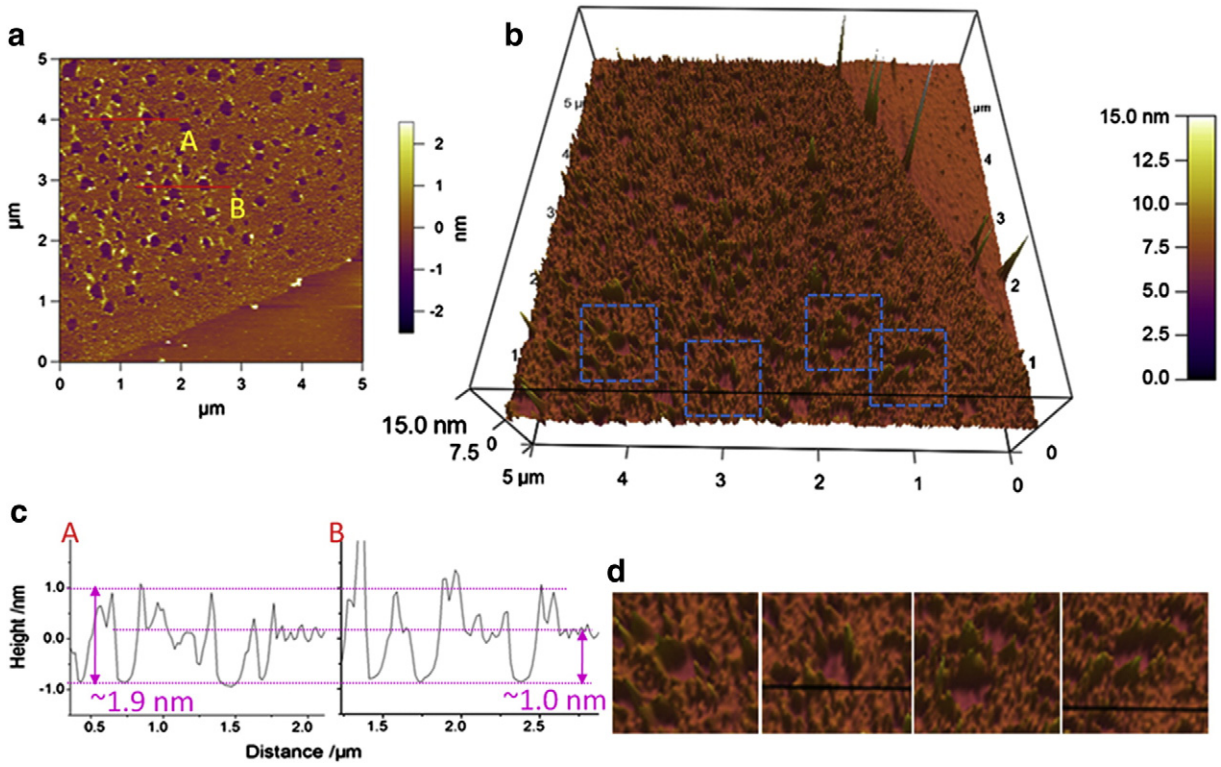

Fig. 4. AFM 2D height mode image (a) and pseudo-3D representation (b) of DOPC monolayer fabricated on rGO surface, with a constant surface pressure of 15 mN m^{-1} during LB deposition. Panel (c) shows height profiles along the red lines in panel (a), marked with (A) and (B), respectively. The average height of the peaks surrounding pores is 1.856 nm, while that of the flatlands is 1.009 nm. The purple dotted lines are added for eye direction. Panel (d) shows zoom-in views of the regions marked with blue dotted squares in panel (b).

average height of 1.01 ± 0.05 nm. However, for the DPPC system, something different happens. In apparent contradiction to the membrane fabricated under 32 mN m^{-1}, the DPPC monolayer on rGO surface lost its continuity and pores were obviously distinguishable. Moreover, on the other regions besides the pores, a large number of small peaks distribute homogeneously over the DPPC′@rGO film surface, with an

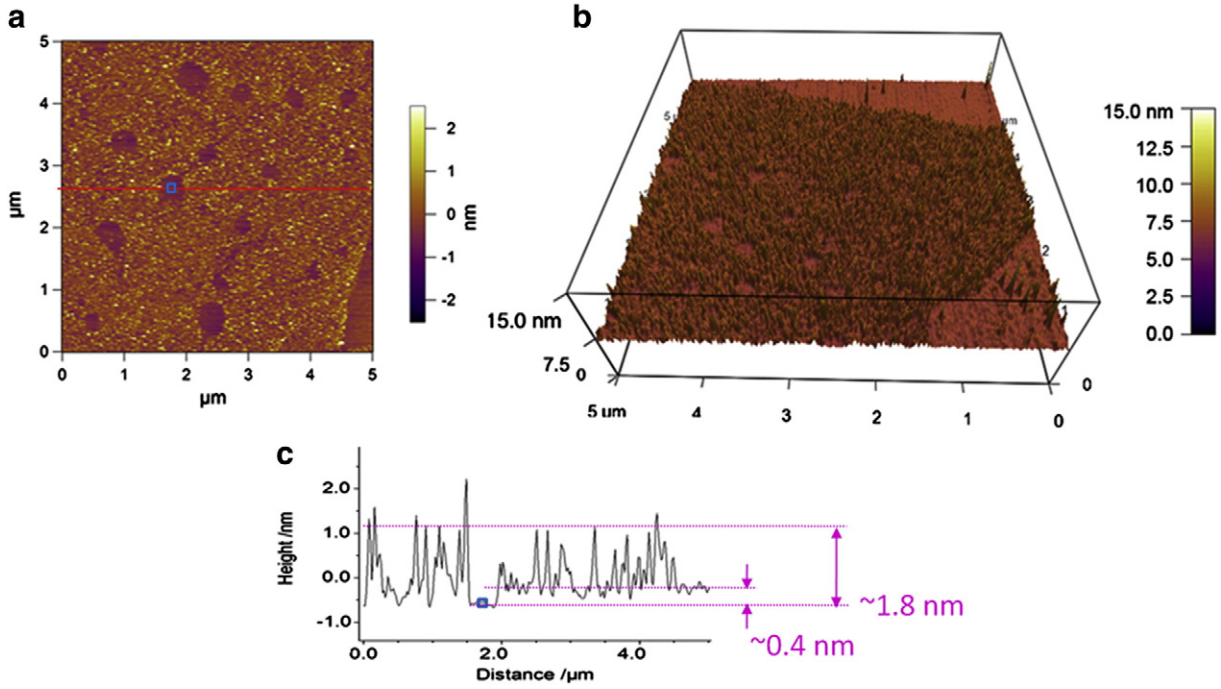

Fig. 5. AFM 2D (a) and 3D (b) representations of DPPC monolayer supported on rGO surface. (c) Height profile along the red line in panel (a). The surface pressure during film deposition was kept at 15 mN m^{-1}.

average height of 1.790 nm. Further explanations would be made in the Discussion section.

3.4. The melting transition in rGO-supported two-component lipid systems of DOPC and DPPC

Several reports have shown that the coexistence of two lipid phases in cell membranes is important in performing various biological functions including material transport, signal transduction, and providing binding sites for pathogens [36]. In our experiments, the mixed DOPC/DPPC monolayer, with a molar ratio of 1:1, was deposited on rGO surface by the same LB technique at a surface pressure of 32 mM m^{-1}. Fig. 6a shows the surface topography of the composite film as prepared. On the naked mica surface without rGO covering, phase separation obviously occurred. The gel and liquid phase domains are unambiguously separated, being similar to what has been reported previously [28]. However, on the rGO region, the size of the phase separation domains is much smaller, and it is difficult to separate a gel domain from the adjacent liquid ones. In other words, the distribution of DOPC and DPPC molecules looks more homogeneous than that on the neat mica surface. In addition, holes are prominently distinguishable, surrounded by a pronounced circle of high molecules which are supposed to be DOPC lipids. This result indicates that the association of rGO with lipid tails has significantly influenced the condition of the tails and even constrained the movement and assembly of lipids on rGO surface. To further confirm the influence of the substrate association, we increased the temperature of the system to 60 °C, being much above the melting temperature of DPPC (41 °C for free bilayer), and maintained for 2 h before AFM analysis. It is observed in Fig. 6b that, the gel and liquid phase separation phenomenon of the lipid monolayer mixtures on naked mica surface became obscure and even some small regions of DPPC domain fused together with that of DOPC. However, for the film on rGO surface, no much change occurred. Moreover, for the high DOPC molecules around pores, neither height nor position of them has changed. The lipid tails of DPPC are supposed to become much more disordered at 60 °C than that at room temperature if phase transition has occurred. This further confirms that the association between lipid tails and rGO substrate significantly constraints the activity such as the main-chain transition of lipids. It regulates the lateral fluidity and phase behavior of the membrane and additional thermal energy might be required to complete the melting and release of the lipid tails [37]. This effect of rGO is in contrast to that of the hydrophilic nanoporous silica layer which reduces the lipid–substrate adhesion and gives rise to enhancement in lateral fluidity of the supported lipid membranes [12].

3.5. Discussion

During the reduction process, the oxygen functional groups of GO are removed leaving only the hydrophobic aromatic plane of graphene with defect pores (Fig. 7a). Strong hydrophobic interaction occurs between the aromatic plane of rGO and the lipid tails. At room temperature, the length of one DOPC molecule from a supported membrane is about 1.82 nm (cf. SI) [38,39]. This length is consistent with the height of the molecules surrounding the pores from a DOPC′@rGO film at 15 mN m^{-1} (1.86 ± 0.1, Fig. 4). Therefore, the circle of high molecules is probably erect DOPC lipids vertical to the substrate surface, with their tails standing against and associated with the edges of the aromatic rings round the pores. On the other regions of the DOPC@rGO film besides pores, the hydrophobic tails of lipids are probably spread over the surface of the aromatic plane [40], leading to a much lowered height of the membrane of 1.01 ± 0.05 nm (Fig. 7c). For the conditions at 32 mN m^{-1}, an increased surface pressure indicates a higher planar number density of the DOPC molecules (Fig. 7b). Therefore, the adjacent lipid tails are more densely packed leading to an increased height of the whole membrane (Fig. 2). An irregular accumulation of lipids might have occurred around the defect holes, resulting in the prominent height of the high molecular circles (from 2 nm to more than 3 nm, Fig. 2e).

For the DPPC film at 15 mN m^{-1}, the lipid molecules are sparsely distributed and cannot form a continuous membrane over the surface of rGO, including pores. There is a height difference of 1.79 nm between the holes and the other regions of the DPPC′@rGO film. This value is much larger than the thickness of a single layer of rGO sheet (0.5 nm) which indicates that the arrangement of lipids within the pores is different from those on rGO surface. Moreover, the average height of the bottom plane of the DPPC′@rGO film is 0.4 nm relative to that of the bottom pore vacancy (Fig. 5c), being close to the thickness of an rGO sheet. As a result, it can be inferred that there is no lipid located within pores and the bottom of pore vacancies can be taken as the “sea level” for the

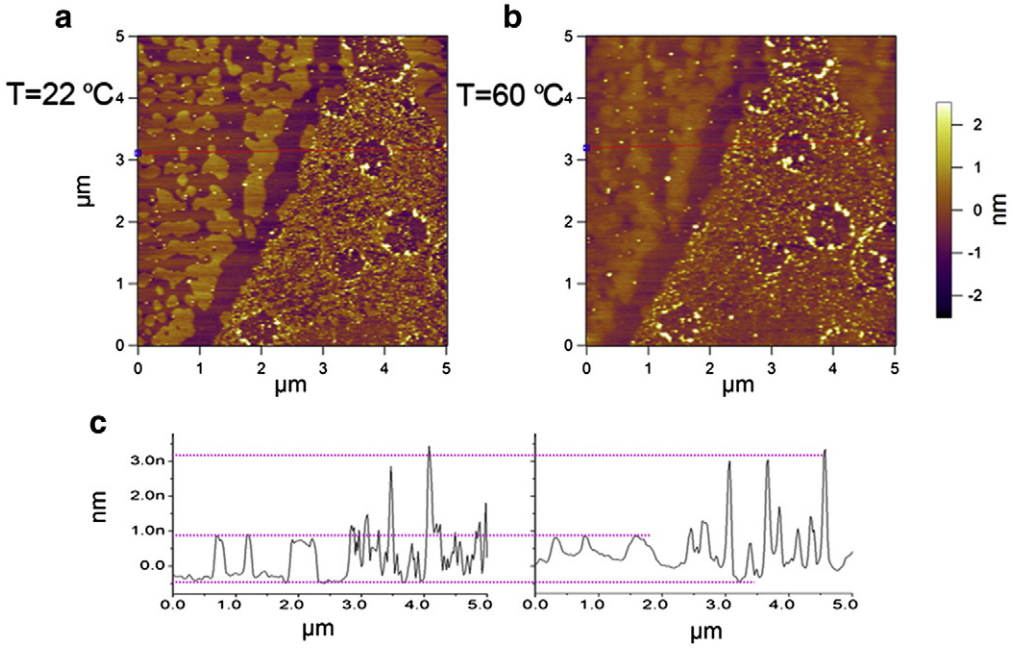

Fig. 6. (a) AFM image of a monolayered membrane composed of DOPC and DPPC mixtures, on an rGO partly covered mica surface. (b) The temperature of the system was elevated to 60 °C and stabilized for 2 h before AFM scanning. Panel (c) shows height profiles along the red lines in panels (a) and (b).

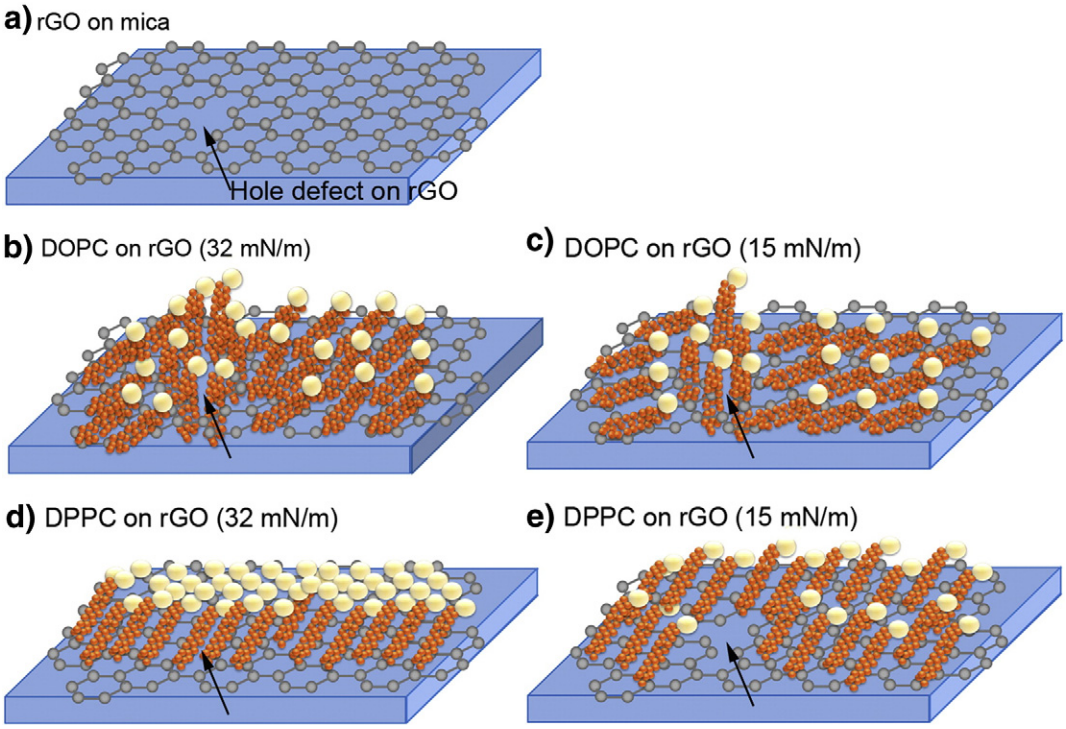

Fig. 7. Schematics of the distributions of DOPC and DPPC molecules on mica-supported rGO surfaces (with defect holes) at different surface pressures of 32 and 15 mN m^{-1}, respectively.

height judgment of the other regions of the sample. The lipids on rGO surface (besides pores) are distributed homogeneously (Fig. 7e), with an average height of 1.4 nm in addition to the 0.4 nm rGO support (Fig. 5c). For the conditions at 32 mN m^{-1}, the DPPC tails are parallel oriented and densely packed. A continuous monolayer is assembled with high bending constant and consequently it completely covers the surface of rGO (including those 0.11 μm sized pores, Figs. 3, 7d). For the DPPC molecules, the surface of the rGO substrate is not so flat at molecular level. The roughness on the DPPC@rGO film might be attributed to the strong hydrophobic interactions between lipid tails and aromatic rings of graphene planes.

4. Conclusions

This work demonstrates a variety of morphology and structures of DOPC and DPPC monolayers assembled on supported single-layered rGO sheets composed of hydrophobic aromatic planes with defect holes due to reduction process. The strong association of lipid tails to the aromatic plane of rGO substrate and the phase state of lipids corporately determine the assembly state of the lipid monolayers. At a low surface pressure of 15 mN m^{-1} for the lipid deposition, the defect holes of rGO sheets, which are indistinguishable for the neat rGO sheets under AFM observations, are now pronouncedly amplified on the lipid′@rGO films. Under this condition, the planar area of each DOPC or DPPC molecule is much larger than that within a cell membrane, and the lipids are separated sparsely within the as deposited monolayers. From the experiment it is demonstrated that the DPPC molecules distributed homogeneously over the aromatic region of rGO sheets, with an average height of 1.8 nm (including the ~0.4 nm rGO support), and left the defect holes of rGO sheets empty. For the DOPC monolayers, the lipids spread completely over the rGO surface with their tails associated with the aromatic plane. Due to the strong association between rGO surface and the disordered lipid tails in liquid phase, the height of the monolayer is only 1.0 nm, much lower than that of DPPC. Besides this, a circle of DOPC molecules stands up vertically to the substrate surface around the defect holes of rGO (with an average height of 1.86 nm approaching the length of DOPC molecules within a bilayer), with their tails standing against the edges of the aromatic rings round the holes. However, at an increased surface pressure of 32 mN m^{-1}, which is considered the lateral pressure values in liposomes, the height of the DOPC@rGO film is much increased as the adjacent lipid tails are more densely packed although they are still disordered due to liquid phase. The holes of rGO are probably surrounded by a circle of lipid accumulations (with a height from 2 to larger than 3 nm as shown in Fig. 2e). In contrast, continuous monolayers have formed for the DPPC lipids. They covered the rGO surface including defect holes with their densely packed and parallel oriented tails due to gel phase. To sum up, our results reveal a dramatic effect of the local structure and surface property of rGO sheet on the substrate-directed assembly, lateral fluidity and phase behavior of the supported lipid membrane, which are of fundamental importance in membrane biophysics.

Conflict of interest

The authors declare that there is no conflict of interest.

Acknowledgements

This work was financially supported by the National Science Foundation of China (Nos. 91027040, 31061160496, 21374074, and 21422404), and the National Basic Research Program of China (No. 2012CB821500). B.Y. and K.Y. thank the support of the Natural Science Foundation of Jiangsu Province of China (Nos. BK2012177 and BK20131194). The authors also thank the Small Angle X-ray Scattering Station (BL16B) and X-ray Diffraction Station (BL14B) at Shanghai Synchrotron Radiation Facility (SSRF) for sample characterizations.

Appendix A. Supplementary data

Supplementary data to this article can be found online at http://dx.doi.org/10.1016/j.bbamem.2015.02.018.

References

[1] F. Zhao, Y. Zhao, Y. Liu, X.L. Chang, C.Y. Chen, Y.L. Zhao, Cellular uptake, intracellular trafficking, and cytotoxicity of nanomaterials, Small 7 (2011) 1322–1337.
[2] T.G. Iversen, T. Skotland, K. Sandvig, Endocytosis and intracellular transport of nanoparticles: present knowledge and need for future studies, Nano Today 6 (2011) 176–185.
[3] M. Massignani, C. LoPresti, A. Blanazs, J. Madsen, S.P. Armes, A.L. Lewis, G. Battaglia, Controlling cellular uptake by surface chemistry, size, and surface topology at the nanoscale, Small 5 (2009) 2424–2432.
[4] K. Yang, Y.Q. Ma, Computer simulation of the translocation of nanoparticles with different shapes across a lipid bilayer, Nat. Nanotechnol. 5 (2010) 579–583.
[5] X. Yao, R. Peng, J.D. Ding, Cell-material interactions revealed via material techniques of surface patterning, Adv. Mater. 25 (2013) 5257–5286.
[6] A. Leclerc, D. Tremblay, S. Hadjiantoniou, N.V. Bukoreshtliev, J.L. Rogowski, M. Godin, A.E. Pelling, Three dimensional spatial separation of cells in response to microtopography, Biomaterials 34 (2013) 8097–8104.
[7] C.J. Bettinger, R. Langer, J.T. Borenstein, Engineering substrate topography at the micro- and nanoscale to control cell function, Angew. Chem. Int. Edit. 48 (2009) 5406–5415.
[8] Y.K. Lee, H. Lee, J.M. Nam, Lipid-nanostructure hybrids and their applications in nanobiotechnology, NPG Asia Mater. 5 (2013) e48.
[9] C.V. Kulkarni, Lipid crystallization: from self-assembly to hierarchical and biological ordering, Nanoscale 4 (2012) 5779–5791.
[10] H.M. Ding, Y.Q. Ma, Design maps for cellular uptake of gene nanovectors by computer simulation, Biomaterials 34 (2013) 8401–8407.
[11] E.L. Kendall, V.N. Ngassam, S.F. Gilmore, C.J. Brinker, A.N. Parikh, Lithographically defined macroscale modulation of lateral fluidity and phase separation realized via patterned nanoporous silica-supported phospholipid bilayers, J. Am. Chem. Soc. 135 (2013) 15718–15721.
[12] G. Hong, J.Z. Wu, J.T. Robinson, H. Wang, B. Zhang, H. Dai, Three-dimensional imaging of single nanotube molecule endocytosis on plasmonic substrates, Nat. Commun. 3 (2012) 700.
[13] W.C. Lee, C.H.Y.X. Lim, H. Shi, L.A.L. Tang, Y. Wang, C.T. Lim, K.P. Loh, Origin of enhanced stem cell growth and differentiation on graphene and graphene oxide, ACS Nano 5 (2011) 7334–7341.
[14] H.K. Na, M.H. Kim, J. Lee, Y.K. Kim, H. Jang, K.E. Lee, H. Park, W.D. Heo, H. Jeon, I.S. Choi, Y. Lee, D.H. Min, Cytoprotective effects of graphene oxide for mammalian cells against internalization of exogenous, Nanoscale 5 (2013) 1669–1677.
[15] K. Kostarelos, K.S. Novoselov, Exploring the interface of graphene and biology, Science 344 (2014) 261–263.
[16] S.R. Ryoo, Y.K. Kim, M.H. Kim, D.H. Min, Behaviors of NIH-3 T3 fibroblasts on graphene/carbon nanotubes: proliferation, focal adhesion, and gene transfection studies, ACS Nano 4 (2010) 6587–6598.
[17] X.G. Hu, Q.X. Zhou, Health and ecosystem risks of graphene, Chem. Rev. 113 (2013) 3815–3835.
[18] K. Furukawa, H. Hibino, Self-spreading of supported lipid bilayer on SiO_2 surface bearing graphene oxide, Chem. Lett. 41 (2012) 1259–1261.
[19] A. Ikeda, T. Sue, M. Akiyama, K. Fujioka, T. Shigematsu, Y. Doi, J. Kikuchi, T. Konishi, R. Nakajima, Preparation of highly photosensitizing liposomes with fullerene-doped lipid bilayer using dispersion-controllable molecular exchange reactions, Org. Lett. 10 (2008) 4077–4080.
[20] S.J. Liu, Q. Wen, L.J. Tang, J.H. Jiang, Phospholipid — graphene nanoassembly as a fluorescence biosensor for sensitive detection of phospholipase D activity, Anal. Chem. 84 (2012) 5944–5950.
[21] J. Liu, S. Guo, L. Han, T. Wang, W. Hong, Y. Liu, E. Wang, Synthesis of phospholipid monolayer membrane functionalized graphene for drug delivery, J. Mater. Chem. 22 (2012) 20634–20640.
[22] A. Ikeda, Y. Doi, M. Hashizume, J. Kikuchi, T. Konishi, An extremely effective DNA photocleavage utilizing functionalized liposomes with a fullerene-enriched lipid bilayer, J. Am. Chem. Soc. 129 (2007) 4140–4141.
[23] S. Garcia-Manyes, L. Redondo-Morata, G. Oncins, F. Sanz, Nanomechanics of lipid bilayers: heads or tails? J. Am. Chem. Soc. 132 (2010) 12874–12886.
[24] S. Pei, H.M. Cheng, The reduction of graphene oxide, Carbon 50 (2012) 3210–3228.
[25] B.L. Stottrup, S.L. Veatch, S.L. Keller, Nonequilibrium behavior in supported lipid membranes containing Cholesterol, Biophys. J. 86 (2004) 2942–2950.
[26] M.J. Uline, I. Szleifer, Mode specific elastic constants for the gel, liquid-ordered, and liquid-disordered phases of DPPC/DOPC/cholesterol model lipid bilayers, Faraday Discuss. 161 (2013) 177–191.
[27] C.V. Kulkarni, W. Wachter, G. Iglesias-Salto, S. Engelskirchen, S. Ahualli, Monoolein: a magic lipid? Phys. Chem. Chem. Phys. 13 (2011) 3004–3021.
[28] M.C. Giocondi, D. Yamamoto, E. Lesniewska, P.E. Milhiet, T. Ando, C. Le Grimellec, Surface topography of membrane domains, BBA-Biomembranes 1798 (2010) 703–718.
[29] D.C. Marcano, D.V. Kosynkin, J.M. Berlin, A. Sinitskii, Z. Sun, A. Slesarev, L.B. Alemany, W. Lu, J.M. Tour, Improved synthesis of graphene oxide, ACS Nano 4 (2010) 4806–4814.
[30] Y. Dou, J. Li, B. Yuan, K. Yang, Lipid merging, protrusion and vesicle release triggered by shrinking/swelling of poly(N-isopropylacrylamide) microgel particles, Appl. Surf. Sci. 296 (2014) 95–99.
[31] O. Akhavan, The effect of heat treatment on formation of graphene thin films from graphene oxide nanosheets, Carbon 48 (2010) 509–519.
[32] M. Acik, Y.J. Chabal, A review on thermal exfoliation of graphene oxide, J. Mater. Sci. Res. 2 (2013) 101–112.
[33] R.C. Van Lehn, M. Ricci, P.H. Silva, P. Andreozzi, J. Reguera, K. Voitchovsky, F. Stellacci, A. Alexander-Katz, Lipid tail protrusions mediate the insertion of nanoparticles into model cell membranes, Nat. Commun. 5 (2014) 4482.
[34] T.J. Zwang, W.R. Fletcher, T.J. Lane, M.S. Johal, Quantification of the layer of hydration of a supported lipid bilayer, Langmuir 26 (2010) 4598–4601.
[35] V. Vie, N. Van Mau, E. Lesniewska, J.P. Goudonnet, F. Heitz, C.L. Grimellec, Distribution of ganglioside G_{M1} between two-component, two-phase phosphatidylcholine monolayers, Langmuir 14 (1998) 4574–4583.
[36] A. Debnath, K.G. Ayappa, V. Kumaran, P.K. Maiti, The influence of bilayer composition on the gel to liquid crystalline transition, J. Phys. Chem. B 113 (2009) 10660–10668.
[37] F.M. Thakkar, K.G. Ayappa, Effect of polymer grafting on the bilayer gel to liquid–crystalline transition, J. Phys. Chem. B 114 (2010) 2738–2748.
[38] B. Yuan, L.L. Xing, Y.D. Zhang, Y. Lu, Z.H. Mai, M. Li, Self-assembly of highly oriented lamellar nanoparticle-phospholipid nanocomposites on solid surfaces, J. Am. Chem. Soc. 129 (2007) 11332–11333.
[39] B. Yuan, L.L. Xing, Y.D. Zhang, Y. Lu, Y.Y. Luo, Z.H. Mai, M. Li, Penetration and saturation of lysozyme in phospholipid bilayers, J. Phys. Chem. B 111 (2007) 6151–6155.
[40] R. Zhou, H. Gao, Cytotoxicity of graphene: recent advances and future perspective, WIREs Nanomed. Nanobiotechnol. 6 (2014) 452–474.